Phys. Rev. B **80**, 155458 (2009) http://dx.doi.org/10.1103/PhysRevB.80.155458

Two-dimensional metal-organic coordination networks of Mn-7,7,8,8-tetracyanoquinodimethane(TCNQ) assembled on Cu (100): structural, electronic and magnetic properties

Tsu-Chun Tseng[1], Chensheng Lin[2,a], X.Q. Shi[2], Steven L. Tait[1,3,†,*], Xiong Liu[1], Ulrich Starke[1], Nian Lin[1,4], R.Q. Zhang[2], C. Minot[2,5], M.A. Van Hove[2,‡,*], J.I. Cerdá[6], and Klaus Kern[1,7]

[1] Max Planck Institute for Solid State Research, Heisenbergstrasse 1, D-70569 Stuttgart, Germany

[2] Department of Physics and Materials Science, City University of Hong Kong, Hong Kong, China

[3] Department of Chemistry, Indiana University, Bloomington, Indiana 47405, USA

[4] Department of Physics, The Hong Kong University of Science and Technology, Clear Water Bay, Hong Kong, China

[5] Laboratoire de Chimie Théorique, Université Pierre & Marie Curie, Paris 6, CNRS, UMR7616, Case 137, 4 place Jussieu, Paris, F-75252 Cedex France

[6] Instituto de Ciencia de Materiales de Madrid, ICMM-CSIC, Cantoblanco, 28049 Madrid, Spain

[7] École Polytechnique Fédérale de Lausanne, 1015 Lausanne, Switzerland

Receipt Date: _____

Abstract

A compound two-dimensional monolayer mixing Mn atoms and 7,7,8,8-tetracyanoquinodimethane (TCNQ) molecules was synthesized by supramolecular assembly on a Cu(100) surface under ultra-high vacuum conditions. Its structural, electronic and magnetic properties were analyzed by scanning tunneling microscopy (STM) experiment and theory, low-energy electron diffraction (LEED), x-ray photoemission spectroscopy (XPS) and density functional theory (DFT) calculations. The 2D compound has a long-range ordered square planar network structure consisting of four-fold coordinated Mn centers with a Mn:TCNQ ratio of 1:2. The electronic state analysis revealed a complex charge transfer scenario indicating strong bonding of TCNQ with both the Mn adsorbates and the Cu surface atoms. The calculations reveal that the Mn centers carry a magnetic moment close to 5 μ_B with very weak coupling between adjacent Mn centers.

PACS: 68.37.Ef, 68.43.Bc, 68.43.Fg, 68.43.Hn, 81.16.Fg

I. INTRODUCTION

Organic-based alternatives to conventional magnets, which offer the possibility to form self-organized nanometer-scale structures with novel magnetic properties, have drawn much attention in the past decades [1-5]. Famous examples are charge transfer salts of metal-7,7,8,8-tetracyanoquinodimethane (TCNQ, with molecular structure shown in the inset of Figure 1c). TCNQ is chosen to coordinate with transition metal ions for preparing molecular magnets because large local superexchange interactions between the high spin state of metal ions and organic spin carriers are expected [6,7]. It has been suggested that the magnetic properties of the metal-TCNQ magnets highly depend on the coordination. Therefore it is important to understand the origin of the magnetism of metal-TCNQ compounds on account of their structural and charge transfer characters.

Studies of metal coordination at surfaces offer the distinct advantages of high control over surface composition as well as capabilities for structural determination with atomic/molecular resolution, and magnetism measurements. The high degree of composition control in UHV studies complements well to careful theoretical calculation. A unique way to study metal coordination is through surface-assisted coordination assembly [8-10]. On two-dimensional (2D) surfaces, due to surface confinement, the formation of novel 2D coordination systems has been demonstrated [11-14]. In this article we present results of the assembly of 2-dimensional $Mn(TCNQ)_2$ coordination networks on a Cu(100) surface. By means of a combined study with scanning tunneling microscopy (STM), low-energy electron diffraction (LEED) and density functional theory (DFT) calculations, we identified that single Mn atoms (ions) form well-defined four-fold square-planar coordination with the cyano groups of TCNQ, resulting in ordered 2D square networks epitaxially grown on the Cu(100) surface. XPS and DFT analyses indicate that a charge transfer to the TCNQ molecules occurs from both the Mn centers and surface Cu atoms. In particular, the magnetic moment of the Mn centers is high (4.9 μ_B), with weak interactions between Mn centers.

II. EXPERIMENT

The preparation of samples was carried out in two ultra-high vacuum systems with a base pressure of about 3×10^{-10} mbar. The Cu(100) surface was cleaned by cycles of Ar^+ ion sputtering and annealing at 800 K. TCNQ molecules were deposited on a clean Cu(100) surface by organic molecular beam epitaxy (OMBE) from a Knudsen-cell type evaporator at a sublimation temperature of 370 K. Mn was subsequently deposited by an electron-beam heating evaporator. The substrate was held at 160 K during and between both deposition steps. After deposition, the sample was annealed for 15 minutes at a temperature between 380 K and 420 K before *in-situ* transfer for STM or XPS characterization, which was done with the sample at room temperature.

III. THEORY

In our DFT calculations, the structures were optimized with the VASP package [15,16], which uses a periodic approach with plane waves as basis set. The projected augmented wave method [17] is adopted. The exchange correlation functional was treated within the generalized gradient approximation (GGA) of Perdew and Wang [18] with the Vosko-Wilk-Nusair (VWN) interpolation of the correlation energy [19]. The kinetic energy cutoff was set to 400eV. Five-layer slabs, with 10 Å of vacuum between slabs, were used to simulate the surface. The top three copper layers and all the adsorbate atoms were allowed to relax until the largest force component was smaller than 0.04 eV/Å, while the bottom two copper layers were fixed to the experimental bulk Cu geometry. Integrations in the first Brillouin zone were performed using a Monkhorst-Pack grid of (2x2x1) *k* points. The details of the initial guessed geometries and the supercell employed will be given in the next section.

IV. ANALYSIS

A typical experimental STM topograph of the Mn-TCNQ assembly on Cu(100) is shown in Figure 1a. The lower part of the figure shows Mn-free close-packed TCNQ molecules, characterized and modeled in detail elsewhere [20]. Above this region is a periodic network structure of TCNQ with Mn and voids (interspersed with larger vacancies). The molecular phase converts into the network phase as the Mn is vapor deposited to the surface, i.e., with increasing

Mn coverage. The yield of the Mn-TCNQ network phase is quantitative, indicating very efficient diffusion and mixing of each of the two components on the surface. Two differently oriented domains of the network were observed, as marked by the arrows in Figure 1a, consistent with mirrored domains and differing by an angle of about 16.2°. These domains have distinct organizational chirality, where the two enantiomeric forms differ in the packing of the TCNQ molecules around the Mn center in a pinwheel formation [21]. Due to the C_4 symmetry of the Cu(100) substrate, we also observed the same domains rotated 90°. A high-resolution STM image of the network is shown in Figure 1b, which clearly reveals that the network is composed of inter-connected TCNQ molecules. The corresponding unit cell is marked by the square in Figure 1b, which has a side length of about 1.28 nm. This suggests that the neighboring Mn centers are separated by a distance close to $5a_0$ (a_0 = 2.55 Å, the nearest neighbor distance of the Cu substrate atoms). The LEED pattern shown in Figure 1c indicates a superposition of two square structures oriented by about ±8.1° from the substrate [100] direction. Both STM and LEED imply that the assembled Mn-TCNQ network periodicity can be expressed as a (4, 3 / -3, 4) superstructure matrix with respect to the substrate Cu(100), equivalent to the Wood notation (5x5)R36.9°.

A schematic model is overlaid on a STM topograph in Figure 1b, where each TCNQ molecule is attached to two Mn atoms and each Mn atom is surrounded by four equivalent TCNQ molecules, giving rise to a $Mn(TCNQ)_2$ compound adsorbed on the Cu(100) surface. Based on this model, the optimized structure shown in Figures 1d and e was obtained by DFT calculations. The Mn atoms adsorb at Cu(100) hollow sites. The optimum distance between Mn and the four nearest Cu atoms is 2.98 Å, which is slightly longer than the sum of the covalent radii of Cu (1.32 Å) and Mn (1.61 Å for Mn in high spin state). The copper surface shows little relaxation except that the four copper atoms which bind to the N atoms of TCNQ move outward by 0.20 Å compared to the average height of the other Cu atoms (the flat part) in that layer. The C atoms of the benzene rings are at an average height of 3.32 Å above the average height of the flat part of the first copper layer, while Mn is 0.89 Å below the average height of the benzene C atoms. Two of the cyano groups of the

TCNQ molecules are strongly bent toward the metal surface with the nitrogen atoms binding to the Cu surface atoms with a Cu–N bond of length 2.00 Å. The other two cyano groups bind to two Mn atoms through the N atoms with a Mn-N bond length of 2.15 Å.

We performed XPS characterization to study the charge states of the $Mn(TCNQ)_2$ network. XPS signals are shown in Figure 2a in the N 1s region for a TCNQ powder, a TCNQ monolayer and $Mn(TCNQ)_2$ networks grown on Cu(100) . The main N 1s peak and a shake-up peak of neutral TCNQ powder are at 399.6 and 401.9 eV, respectively [22-25]. The main peak of the TCNQ monolayer is at 398.7 eV, shifted by 0.9 eV to lower binding energy, which indicates charge transfer to TCNQ [23-26]. This suggests that TCNQ molecules readily take electrons from Cu(100) as soon as they adsorb on the substrate. However the N 1s signal of the $Mn(TCNQ)_2$ network is very similar to that of a TCNQ monolayer, indicating no obvious difference in the charge states of nitrogen in these two situations.

Through Bader charge analysis [27] of the DFT optimized geometry, we can gain insight into the charge transfer mechanism by considering the partial systems listed in Table 1; we stress that the trends in such charges are more meaningful than the precise numerical values. The atomic coordinates of the three partial systems are the same as in the full 2TCNQ+Mn/Cu(100) system. In the full system, the TCNQ molecule, serving as electron acceptor, carries a negative charge of −1.38|e|. The Cu and the Mn both contribute to the donation. The charge of Mn is +1.33|e|, which approaches the Mn^{2+} state, whereas the Cu(100) surface is charged to +1.43|e|. In the 2TCNQ+Mn system, we found a transfer of -0.73|e| to each TCNQ from Mn and in the Mn-free 2TCNQ/Cu(100) system, a transfer of -1.12|e| occurs from the copper surface. The charge on the TCNQ in the full 2TCNQ+Mn/Cu(100) system, −1.38|e|, exceeds these values: the charges on the N atoms increase by -0.24|e| for N1 and -0.30|e| for N2 with respect to the pure $(TCNQ)_2$ network, where N1 and N2 bond to Cu and Mn, resp. This charge increase is primarily due to donation from Cu to N1 and from Mn to N2. For the Mn-free 2TCNQ/Cu(100) system, the redistribution is principally localized in the N-Cu bonds, where each N1 atom gains -0.24|e|. For the $Mn(TCNQ)_2$

network in the absence of the Cu substrate, the N2 atoms gain −0.30|e| relative to N in the pure $(TCNQ)_2$ network. This analysis reveals that the charge of the N1 atoms in the Cu-N bonds changes little compared to that of the N2 atoms of Mn-N bonds, which is consistent with the XPS data. This is also consistent with a strong electron donation from both Mn and Cu to the TCNQ, especially to the N atoms. This significant charge transfer is a critical aspect of the system, both for structural arrangement and for determining the electronic configuration, as discussed below.

The geometry of the TCNQ also reveals the effect of the charge transfer. While the successive CC bonds in free TCNQ have alternating long and short distances (cf. the C_0-C_1, C_1-C_2, C_2-C_3 and C_3-C_3 distances listed in Table 2), the structure after adsorption shows in the dianion $TCNQ^{2-}$ species (cf. Table 2) a shortened C_0-C_1 distance, an elongated C_1-C_2 distance and nearly equivalent C_2-C_3 and C_3-C_3 distances within the ring.

The optimized $Mn(TCNQ)_2$/Cu(100) network structure was used to simulate the STM imaging [28], as shown in Fig. 3a. The Mn centers dominate the image and are thus too bright compared to the experimental data of Fig. 1b. After excluding tip effects [29], we ascribed this discrepancy to the fact that the electronic structure of the $Mn(TCNQ)_2$ network is not described accurately by the normal DFT approach. In a system like $Mn(TCNQ)_2$ the electronic correlation effect due to tightly bound and localized *d*-states on the transition metal atoms should be taken into account. An improvement that addresses this issue is the LDA+*U* method [30-32]. In this approach, a Hubbard-like term is added to the DFT Hamiltonian to account for the strong on-site intra-atomic Coulomb repulsion *U*. The parameter *U* describes the energy rise due to placing an extra electron into the *d* level on a particular site, and an additional parameter *J* represents the screened exchange energy. While *U* depends on the spatial extension of the wavefunctions and on screening, *J* is an approximation to the Stoner exchange parameter and is almost constant with a value near 1 eV. We applied the DFT + *U* approach based on the work of Dudarev et al [32], which uses the single effective parameter *U-J* (or $U_{\text{eff}} = U-J$). As a rough approximation [33], we set the U_{eff} value for Mn to 4.2eV. Fig. 3b shows the STM image produced by the parameter fitting to the projected

density of states (PDOS) with the Hubbard *U* correction. We see that the signal of the Mn centers is significantly reduced relative to that of the TCNQ molecules, which agrees much better with the experimental images than without a Hubbard *U* correction.

The LDA + *U* treatment pushes the unoccupied states to higher energy, increasing the energy gap. As shown in Figs. 3c and 3d, with the correction U_{eff} = 4.2eV, the gap between the occupied and unoccupied majority-spin states is enlarged from 1.9eV to 4.1eV. Without the Hubbard *U* correction, there is a large contribution from Mn 3*d* minority-spin states in the energy range of ±1 eV around the Fermi level, which results in the Mn atom contributing significantly to the tunneling current and appearing very bright in the simulated STM image. After applying the Hubbard *U* correction with U_{eff} = 4.2eV, the Mn 3*d* orbital DOS above/below the Fermi level is shifted up/down in energy in agreement with the U exclusion effect, forming a large energy gap. As shown in Fig. 3d, the TCNQ levels are not affected by this shift, so that the abovementioned charge transfers are only negligibly modified. As a result, the PDOS of Mn 3*d* is smaller than the PDOS of TCNQ at the Fermi level, making the Mn atom in the simulated STM less bright than without Hubbard correction.

We next address the magnetic moment in this structure, adopting the convention, frequently used in the literature [30], that the spin magnetic moment μ is the difference in occupation numbers between majority-spin and minority-spin orbitals, in units of μ_B. We found that, when U_{eff} = 4.2eV, the magnetic moment for Mn atom reaches μ = 4.9 μ_B, which is close to the nominal value of 5 for a Mn^{2+} ion in a high spin state, in the absence of a significant crystal field effect. This is visible through the PDOS shown in figure 4, which shows the five Mn d orbitals that all contribute to the spin: the d_{xy} and d_{x2-y2} orbitals in Fig 4a and the other three d orbitals in Fig 4b displayed with another scale (note that the d_{xz} and d_{xz} orbitals are equivalent). The Fermi level is determined by the copper orbitals, which do not contribute to the spin polarization. In figure 4b, three peaks of the TCNQ levels – a sharp peak at E_{Fermi}-3.5eV (2e), a family of peaks at E_{Fermi}-2.5eV (4e) and a sharp peak E_{Fermi}-0.5eV (2e) – correspond to four Cu-N bonds and do not contribute to the spin. Figure

4b displays the PDOS on the 4 N atoms adjacent to the cyano groups close to Cu which are the dominant contribution. We can therefore interpret the magnetization as resulting from a Mn^{2+} ion interacting with a TCNQ dimer dianion, $[TCNQ^{2-}]_2$. Our calculations confirm that the spin is strongly localized on the Mn.

Finally, we searched for a periodic spin arrangement and found that, using the Mn+2TCNQ model with three Cu layers, the ferromagnetic (FM) arrangement and the antiferromagnetic (AFM) arrangement have essentially the same energy (differing by only 5 meV). Therefore, the spin coupling between adjacent Mn ions is small and each Mn ion may be regarded as an independent magnet.

V. CONCLUSIONS

We have performed a combined experimental and theoretical study of a self-assembled Mn-TCNQ network on Cu(100) under ultra-high vacuum conditions, using STM, LEED, XPS and DFT calculations. The STM and LEED experiments reveal a highly-ordered (5x5)R36.9° periodic structure . Each unit cell contains two intact flat-lying TCNQ molecules and one Mn atom, which connects four TCNQ molecules together. Theory indicates significant charge transfer in the strong Mn-N bonding within the 2D network, as well as in Cu-N bonds that pin the network to the Cu(100) surface. The calculations reveal that the Mn centers carry a magnetic moment of 4.9 μ_B, with weak coupling between adjacent Mn magnetic moments. Together, these results characterize a two-dimensional metal-organic system formed by a highly efficient self-assembly process which consists of well-ordered independent magnetic metal centers.

Acknowledgements

This work was supported in part by Hong Kong RGC Grant No. CityU 102408, and by the CityU Centre for Applied Computing and Interactive Media. All of the experimental work was performed at MPI Stuttgart and was supported by the European Science Foundation (ESF) EUROCORES-SONS2 program FunSMARTs II. JIC acknowledges financial support

from the Spanish MICINN under contract no. MAT2007-66719-C03-02. CM is grateful to the French Consulate General in Hong Kong and Macau for financial support.

References

[a] Current address: Fujian Institute of Research on the Structure of Matter, Chinese Academy of Sciences, Fuzhou, China.

* To whom correspondence may be addressed.

† Electronic address: tait@indiana.edu

‡ Electronic address: vanhove@cityu.edu.hk

1. O. Kahn, Molecular Magnetism (VCH, New York, 1993).
2. J. S. Miller, Inorg. Chem. **39**, 4392 (2000).
3. J. S. Miller, and A. J. Epstein, MRS Bull. **25**, 21 (2000).
4. S. Ferlay, T. Mallah, R. Ouahes, P. Veillet, and M. A. Verdaguer, Nature **378**, 701 (1995).
5. P. Gambardella, S. Stepanow, A. Dmitriev, J. Honolka, F. de Groot, M. Lingenfelder, S. Sen Gupta, D. D. Sarma, P. Bencok, S. Stanescu, S. Clair, S. Pons, N. Lin, A. P. Seitsonen, H. Seitsonen, J. V. Barth, and K. Kern, Nature Materials **8**, 189 (2009).
6. R. Clerac, et al. Chem. Mater. **15**, 1840 (2003).
7. G. Long, and R. D. Willett, Inorg. Chim. Acta **313**, 1 (2001).
8. N. Lin, S. Stepanow, M. Ruben, and J. V. Barth, Topics in Current Chemistry, **287**, 1, (2009)
9. N. Lin, S. Stepanow, F. Vidal, K. Kern, S. Alam, S. Strömsdörfer, S. Dremov, P. Müller, A. Landa, and M. Ruben, Dalton Trans. 2794 (2006).
10. J. V. Barth, G. Costantini, and K. Kern, Nature **437**, 671 (2005).
11. S. L. Tait, Y. Wang, G. Costantini, N. Lin, A. Baraldi, F. Esch, L. Petaccia, S. Lizzit, and K. Kern, J. Am. Chem. Soc. **130**, 2108 (2008).
12. A. Langner, S.L. Tait, N. Lin, C. Rajadurai, M. Ruben, and K. Kern, Proc. Nat. Acad. Sci. USA **104**, 17927 (2007).

13. S. Stepanow, N. Lin, D. Payer, U. Schlickum, F. Klappenberger, G. Zoppellaro, M. Ruben, H. Brune, J.V. Barth , and K. Kern, Angew. Chem. Int. Ed. **46**, 710 (2007).

14. S. Stepanow, N. Lin, J.V. Barth, and K. Kern, J. Phys. Chem. B **110**, 23472 (2006).

15. G. Kresse, and J. Hafner, Phys. Rev. B **47**, 558 (1993); **49**, 14251 (1994).

16. G. Kresse, and J. Furthmüller, Comput. Mater. Sci. **6**, 15 (1996); Phys. Rev. B **54**, 11169 (1996).

17. P. E. Blöchl, Phys. Rev. B **50**, 17953 (1994); G. Kresse, and J. Joubert, Phys. Rev. B **59**, 1758 (1999).

18. J. P. Perdew, J. A. Chevary, S. H. Vosko, K. A. Jackson, M. R. Pederson, D. J. Singh, and C. Fiolhais, Phys. Rev. B **46**, 6671 (1992).

19. S. H. Vosko, L. Wilk, and M. Nusair, Can. J. Phys. **58**, 1200 (1980).

20. T.-C. Tseng, C. Urban, Y. Wang, R. Otero, S. L. Tait, M. Alcamí, D. Écija, M. Trelka, J. M. Gallego, N. Lin, M. Konuma, U. Starke, A. Nefedov, C. Wöll, M. Á. Herranz, F. Martín, N. Martín, K. Kern, and R. Miranda, *submitted* (2009).

21. V. Humblot, S. M. Barlow, and R. Raval, Prog. Surf. Sci. **76**, 1 (2004).

22. S.K. Wells, J. Giergel, T.A. Land, J. M. Lindquist, and J. C. Hemminger, Surf. Sci. **257**, 129 (1991).

23. J. Giergiel, S. Wells, T.A. Land, and J. C. Hemminger, Surf. Sci. **255**, 31 (1991).

24. W. D. Grobman, R. A. Pollak, D. E. Eastman, E. T. Maas, Jr., and B. A. Scott, Phys. Rev. Lett. **32**, 534 (1974).

25. M. Higo, T. Futagawa, M. Mitsushio, T. Yoshidome, and Y. Ozono, J. Phys. Chem. B **107**, 5871 (2003).

26. T. Patterson, J. Pankow, and N. R. Armstrong, Langmuir **7**, 3160 (1991).

27. W. Tang, E. Sanville, and G. Henkelman, J. Phys.: Condens. Matter **21**, 084204 (2009).

28. We simulated STM images by using the GREEN code (ref. 34), which is based on a Green's function representation and employs a linear combination of atomic orbitals. The

extended Hückel theory (EHT) was used to compose the semi-empirical Hamiltonian. First we fit the EHT parameters to reproduce the DFT density of states (DOS) of the sample and tip. Then an infinite system composed of two semi-infinite blocks for the tip and the sample was constructed, using the parameterized EHT to simulate the STM image. The W tip has a pyramidal shape with the W(110) plane parallel to the surface, although the exact tip shape and composition used in the experiment are not known.

29. We also tried to use Cu as the tip material since it is possible that the extreme tip atom is a copper atom. However, the simulated STM images are similar to the W tip results.
30. V. I. Anisimov, J. Zaanen, and O. K. Andersen, Phys. Rev. B **44**, 943 (1991).
31. A. I. Liechtenstein , V. I. Anisimov, and J. Zaanen, Phys. Rev. B **52**, 5467 (1995).
32. S. L. Dudarev , G. A. Botton, S. Y. Savrasov, C. J. Humphreys, and A. P. Sutton, Phys. Rev. B **57**, 1505 (1998).
33. A. Rohrbach , J. Hafner, and G. Kresse, J. Phys.: Condens. Matter **15**, 979 (2003).
34. J. Cerdá, M. A. Van Hove, P. Sautet, and M. Salmeron, Phys. Rev. B **56**, 15885 (1997).
35. K. Ueda, T. Sugimoto, S. Endo, N. Toyota, M. Kohama, K. Yamamoto, Y. Suenaga, H. Morimoto, T. Yamaguchi, M. Munakata, N. Hosoito, N. Kanehisa, Y. Shibamoto, Y. Kai, Chem. Phys. Letters **261**, 295 (1996)

Table captions:

Table 1. Bader charge analysis in units of |e| in the different calculated models.

Table 2. Bond distances (Å) in TCNQ, as neutral monomer, negatively charged dianion dimer, Mn-$[TCNQ]_2$/Cu(100) and $TCNQH_4$ (the theoretical basis set used is specified between parentheses).

Figure captions:

Figure 1. (a) STM topograph of the Mn-TCNQ assembly on a Cu (100) surface. (b) High-resolution STM topograph of the $Mn(TCNQ)_2$ network. (c) LEED pattern of the $Mn(TCNQ)_2$ network. Inset: Chemical structure of the molecule TCNQ. (d) and (e) Top and side views of the DFT-optimized structure of the $Mn(TCNQ)_2$ network on the Cu(100) surface Color code: Cu red, C gray, N blue, H white, Mn purple.

Figure 2. XPS N1s signal of TCNQ powder, TCNQ monolayer grown on Cu(100) and $Mn(TCNQ)_2$ networks grown on Cu(100).

Figure 3. (a) Simulated STM image at 0.5 V using DFT results for the $Mn(TCNQ)_2$ network structure on Cu(100). (b) Same as (a) but with a Hubbard U correction, U_{eff} = 4.2eV. (c, d) Spin-projected densities of states (PDOS) for Mn and TCNQ adsorbed on a Cu(100) surface, calculated with VASP without Hubbard U (c), and using U_{eff} = 4.2eV (d). The PDOS of Mn is indicated in blue. The PDOS of the TCNQ molecules is indicated as red solid lines, with positive (negative) values for the majority-spin (minority-spin) PDOS.

Figure 4. (a) The PDOS of the top copper layer, of the TCNQ molecule and of the Mn d_{xz} and d_{x2-y2} orbitals. (b) The PDOS of the Mn d_{xz} (d_{yz}) and d_{z2} orbitals and of the 4 N atoms adjacent to the cyano groups close to Cu. Note that the PDOS of the d_{xz} and d_{yz} orbitals are equal.

Table 1.

System	per TCNQ	Mn	Cu(100)	N1[a]	N2[a]
2TCNQ	0			-1.00	
2TCNQ/Cu(100)	-1.12	N/A	+2.25	-1.24	-1.10
2TCNQ+Mn	-0.73	+1.46	N/A	-1.04	-1.31
2TCNQ+Mn/Cu(100)	-1.38	+1.33	+1.43	-1.24	-1.30

[a] N1 are N atoms that bond to Cu, while N2 are N atoms that bond to Mn in the full system.

Table 2.

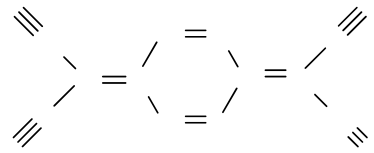	C_0N_{Cu}	C_0-C_1	C_1-C_2	C_2-C_3	C_3-C_3
TCNQ (B3LYP/3-21G) [35]	1.17	1.42	1.39(1.37)	1.45(1.45)	1.355(1.35)
dianion dimer (B3LYP/3-21G)	1.18	1.40	1.475	1.42	1.39
Mn-[TCNQ] $_2$/Cu(100)	1.18	1.38	1.47	1.39	1.41
$TCNQH_4$ (B3LYP/3-21G)	1.22	1.37	1.50	1.40	1.39

Figure 1.

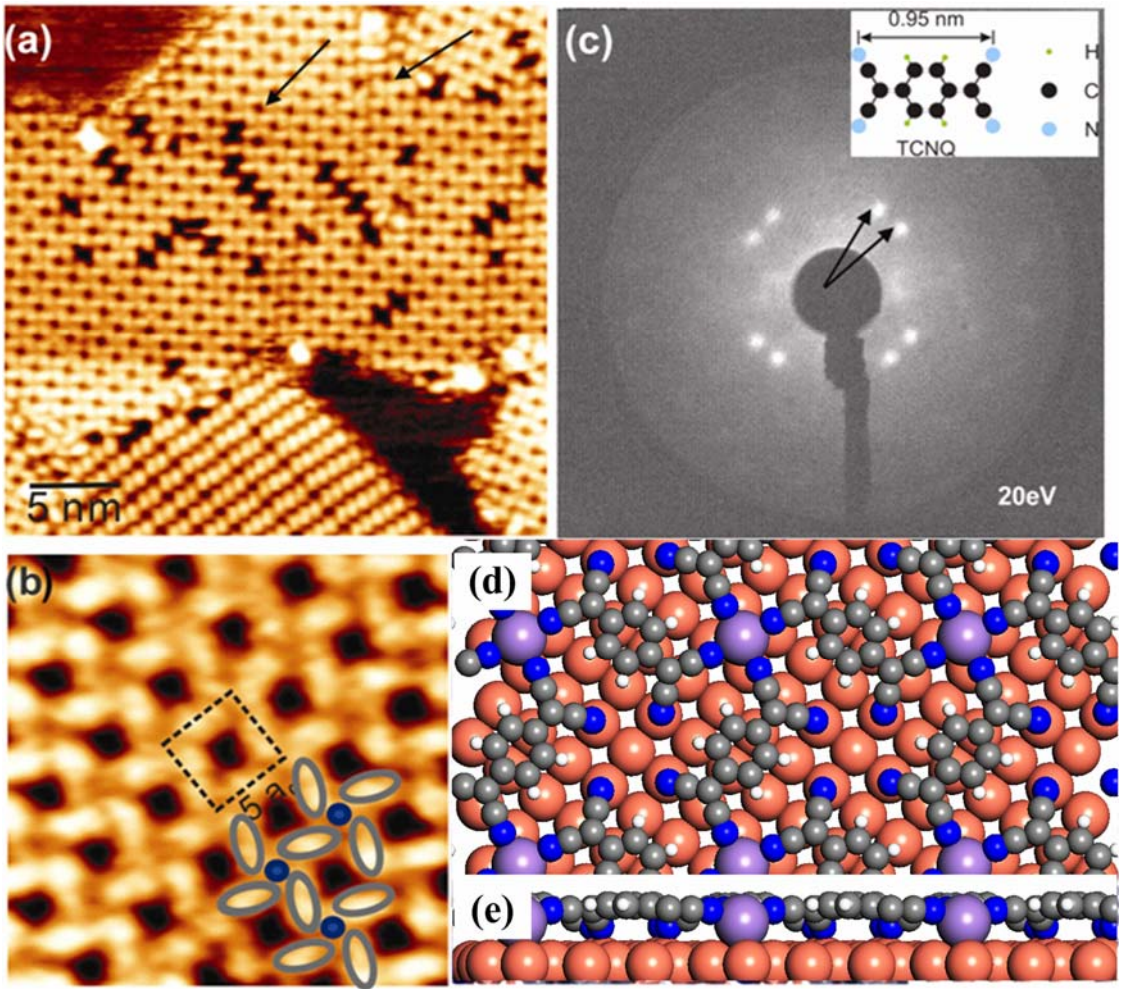

Figure 2.

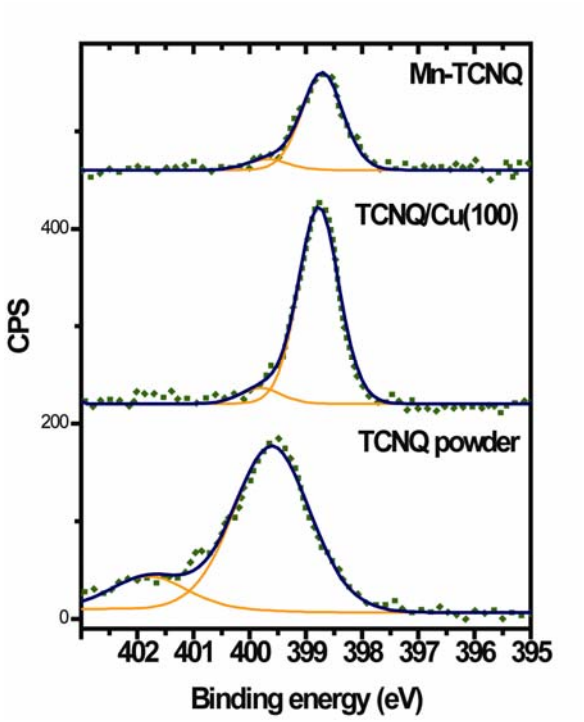
Mn-TCNQ
TCNQ/Cu(100)
TCNQ powder
CPS
400
200
0
402 401 400 399 398 397 396 395
Binding energy (eV)

Figure 3.

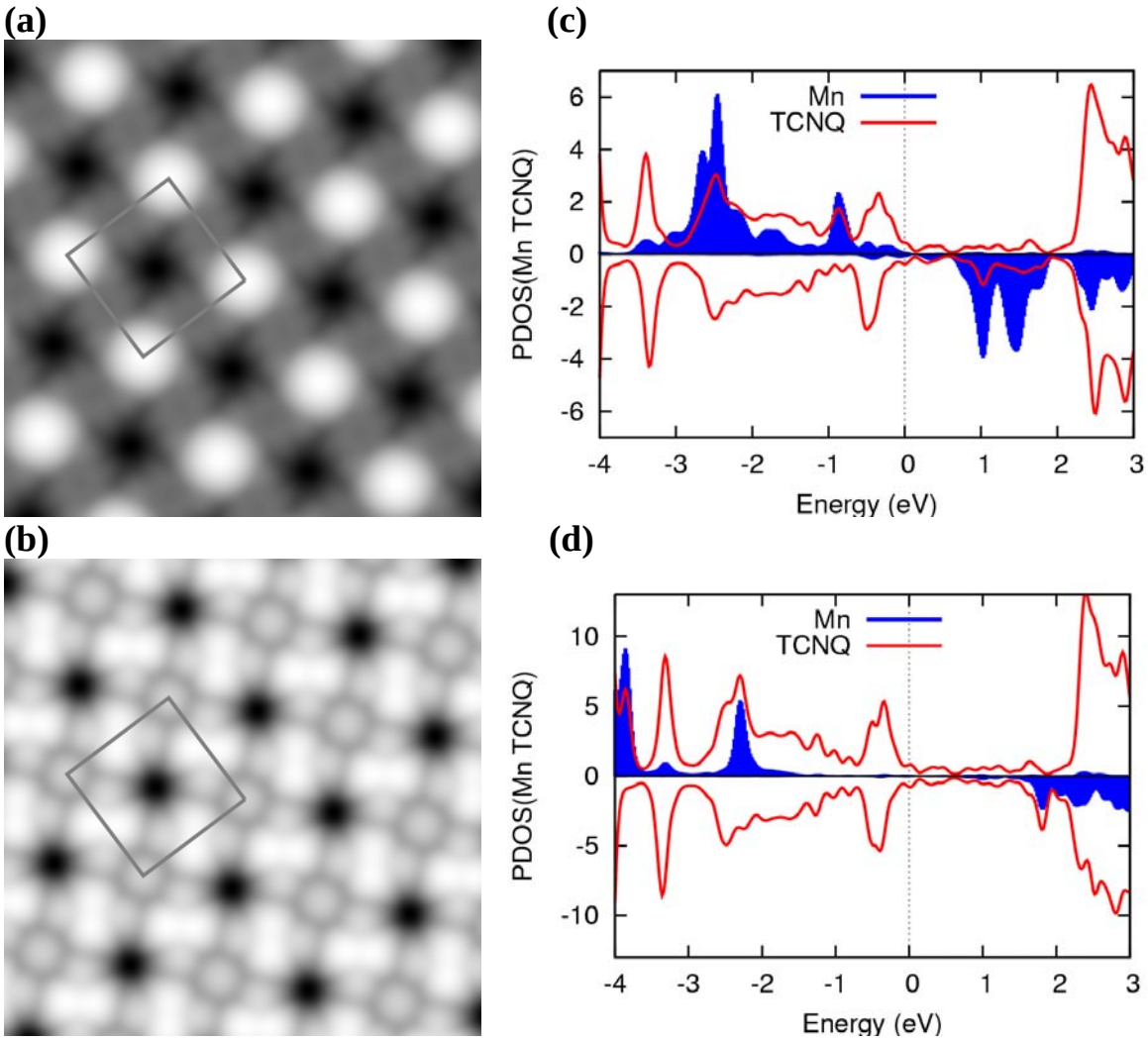

Figure 4.

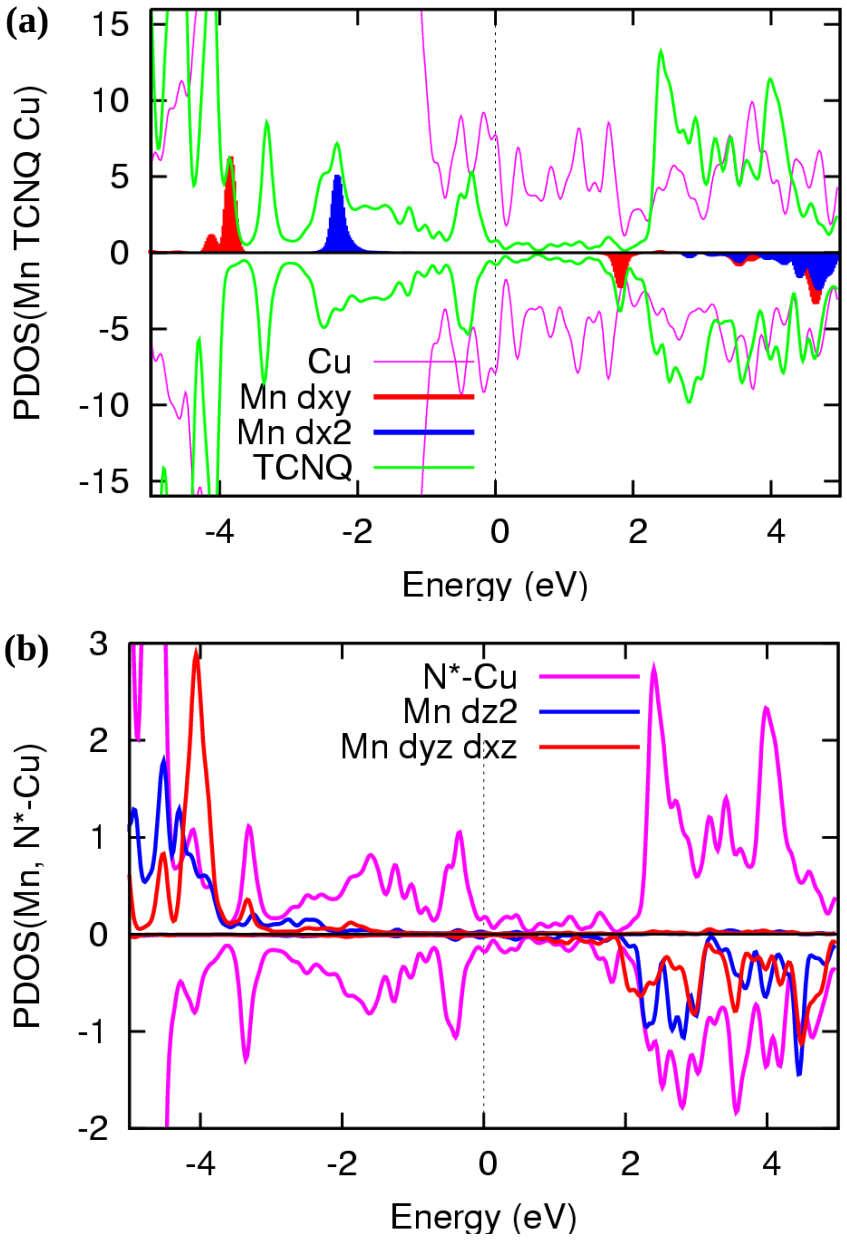
(a)
PDOS(Mn TCNQ Cu)
15
10
5
0
-5
-10
-15
-4
-2
0
2
4
Energy (eV)
Cu
Mn dxy
Mn dx2
TCNQ
(b)
PDOS(Mn, N*-Cu)
3
2
1
0
-1
-2
-4
-2
0
2
4
Energy (eV)
N*-Cu
Mn dz2
Mn dyz dxz